Sterol 14-alpha demethylase (CYP51) activity in Leishmania donovani is likely dependent upon cytochrome P450 reductase 1

Tulloch, Lindsay; Tinti, Michele; Wall, Richard; Weidt, Stefan K.; Corpas Lopez, Victoriano; Dey, Gourav

Published in:
PLoS Pathogens

DOI:
10.1371/journal.ppat.1012382

Publication date:
2024

Sterol 14-alpha demethylase (CYP51) activity in *Leishmania donovani* is likely dependent upon cytochrome P450 reductase 1

Lindsay B. Tulloch[1], Michele Tinti[1], Richard J. Wall[*1], Stefan K. Weidt[2], Victoriano Corpas-Lopez[1], Gourav Dey[1], Terry K. Smith[3], Alan H. Fairlamb[1], Michael P. Barrett[2,4] and Susan Wyllie[1#]

[1]Wellcome Centre for Anti-Infectives Research, School of Life Sciences, University of Dundee, Dow Street, Dundee, United Kingdom

[2]Glasgow Polyomics, College of Medical, Veterinary and Life Sciences, University of Glasgow, Garscube Estate, Bearsden, Glasgow, United Kingdom

[3]Biomedical Sciences Research Complex, University of St Andrews, St Andrews, United Kingdom

[4]School of Infection & Immunity, College of Medical, Veterinary and Life Sciences, University of Glasgow, Glasgow, United Kingdom

[*]Current address: London School of Hygiene and Tropical Medicine, Keppel St, London, United Kingdom

[#]**Corresponding author:** Susan Wyllie (s.wyllie@dundee.ac.uk)

Keywords: Drug resistance, mechanism of action, *Leishmania*, visceral leishmaniasis, sterol metabolism, P450 reductase and sterol 14-alpha demethylase (CYP51)

Abstract

Liposomal amphotericin B is an important frontline drug for the treatment of visceral leishmaniasis, a neglected disease of poverty. The mechanism of action of amphotericin B (AmB) is thought to involve interaction with ergosterol and other ergostane sterols, resulting in disruption of the integrity and key functions of the plasma membrane. Emergence of clinically refractory isolates of *L*. *donovani* and *L. infantum* is an ongoing issue and knowledge of potential resistance mechanisms can help to alleviate this problem. Here we report the characterisation of four independently selected *L. donovani* clones that are resistant to AmB. Whole genome sequencing revealed that in three of the moderately resistant clones, resistance was due solely to the deletion of a gene encoding C24-sterol methyltransferase (SMT1). The fourth, hyper-resistant resistant clone (>60-fold) was found to have a 24 bp deletion in both alleles of a gene encoding a putative cytochrome P450 reductase (P450R1). Metabolic profiling indicated these parasites were virtually devoid of ergosterol (0.2% versus 18% of total sterols in wild-type) and had a marked accumulation of 14-methylfecosterol (75% versus 0.1% of total sterols in wild-type) and other 14-alpha methylcholestanes. These are substrates for sterol 14-alpha demethylase (CYP51) suggesting that this enzyme may be a *bona fide* P450R specifically involved in electron transfer from NADPH to CYP51 during catalysis. Deletion of P450R1 in wild-type cells phenocopied the metabolic changes observed in our AmB hyper-resistant clone as well as in CYP51 nulls. Likewise, addition of a wild type P450R1 gene restored sterol profiles to wild type. Our studies indicate that P450R1 is essential for *L. donovani* amastigote viability, thus loss of this gene is unlikely to be a driver of clinical resistance. Nevertheless, investigating the mechanisms underpinning AmB resistance in these cells provided insights that refine our understanding of the *L. donovani* sterol biosynthetic pathway.

Author summary

The antifungal drug, amphotericin B, is also used in the treatment of visceral leishmaniasis, a potentially lethal parasitic disease infecting the specialised immune cells (macrophages) in the liver, spleen, and bone marrow. Treatment failures due to emerging drug resistance are a significant concern. Using a combination of genetic and biochemical approaches, we have confirmed the mechanisms by which these parasites become less sensitive to treatment with amphotericin B. In addition, we have identified a novel mechanism involving loss of a key enzyme (cytochrome P450 reductase 1) in the biosynthetic pathway to ergosterol, an important lipid component of the parasite's plasma membrane. These studies increase our fundamental understanding of this important metabolic pathway and provide information that may be exploited to develop novel therapeutic strategies to combat this killer disease.

Introduction

Leishmaniasis is a neglected tropical disease caused by infection with protozoan parasites of the *Leishmania* genus and transmitted through the bite of infected sandflies. There are an estimated 700,000-1,000,000 new cases annually, with the vast majority of infections occurring in the Americas, the Middle East, Central Asia, and East and West Africa [1]. Thus, leishmaniasis disproportionately affects some of the most impoverished parts of the world. Disease typically presents in three clinical forms depending upon the species of parasite responsible for the infection. The most common form is cutaneous leishmaniasis, which results in ulcers at the site of the sandfly bite that are self-healing but can leave life-long scars. Muco-cutaneous leishmaniasis, although not life-threatening, leads to partial or complete destruction of the mucous membranes of the nose, mouth, and throat. Visceral leishmaniasis (VL), resulting from systemic infection with *Leishmania donovani* or *L. infantum*, is the most severe form of the disease. It is characterised by bouts of fever, weight loss, anaemia, hepatosplenomegaly and, if left untreated, is usually fatal [1].

In the absence of a viable vaccine, treatment of the various forms of leishmaniasis is almost entirely reliant upon chemotherapy. At present, four drugs are in regular clinical use, namely pentavalent antimonials, miltefosine, paromomycin and amphotericin B (reviewed in detail in [2] and [3]). Treatment selection is based on a number of factors including parasite species, prevalence of resistance to specific drugs in the geographical area and available resources. Unfortunately, each one of these drugs suffers from issues that make them far from ideal including severe toxic side effects [4, 5], acquired drug resistance [6] and prolonged treatment regimens [7]. Antimonials, such as sodium stibogluconate, have been used for the treatment of leishmaniasis since the 1940s but are associated with severe toxicity. While antimonials remain a front-line therapy for VL in East Africa, high levels of treatment failure associated with drug resistance now preclude the use of these drugs in India [8]. Miltefosine, the only orally bioavailable antileishmanial, is teratogenic and therefore cannot be prescribed to women of child-bearing age. Furthermore, the prolonged half-life of miltefosine (7 days) is

considered to significantly increase the resistance potential of this alkylphosphocholine drug [2]. Indeed, 20% of patients treated with miltefosine during a cohort study of VL patients in Nepal relapsed [7], although a direct role for parasite resistance in these treatment failures was not established. Paromomycin was recently approved for the treatment of VL following successful phase II clinical trials in India [9, 10], however, paromomycin performed less well in similar trials in Sudan [11, 12].

Liposomal amphotericin B (AmB) is considered the standard of care for VL in many countries. Commonly, this polyene antibiotic is administered through multiple intravenous infusions (15 in total) over a 30-day period. The high cost of this treatment, coupled with associated toxicity, has driven the implementation of reduced treatment regimens [13]; however, there are concerns that these shortened regimes may be contributing to emerging amphotericin B resistance in India [14, 15]. AmB belongs to a family of glycosylated macrolactone polyene antibiotics that demonstrate potent antifungal activity. The mechanism of action of these polyenes is thought to involve selective binding to ergostane-type rather than cholestane-type membrane sterols [16], leading to the formation of pores that disrupt cellular homeostasis and ultimately lead to cell death [17]. However, shorter polyene sterols thought to be incapable of pore-formation also display fungicidal activity leading to the suggestion that ergosterol sequestration rather than pore formation may be responsible for cell death [18, 19]. One favoured model involves AmB forming extra-membranous sponge-like aggregates that extract ergosterol from lipid bilayers [20, 21]. The selective toxicity of AmB for fungi and *Leishmania* may depend on the different extraction rates for ergosterol and related sterols in the membranes of these pathogens, in contrast to mammalian cells where cholesterol is the major sterol [22].

Multiple studies in both fungi and *Leishmania* have linked a plethora of mutations in the enzymes of the ergosterol biosynthetic pathway to AmB resistance (**Figure 1**) [23-26]. Many of the mutations are thought to reduce the levels of ergosterol in the membranes of these organisms. Altered antioxidant defences have also been associated with modest resistance [26-28] suggesting that oxidative stress may also play a role in the cytocidal activity of this

polyene macrolide. Indeed, previous studies have demonstrated that AmB has the ability to auto-oxidise [29]. Collectively, these studies indicate that the mechanisms of action and mechanisms underpinning AmB resistance may be more complex than generally accepted. For drugs used in a clinical setting, it is vital that there is a comprehensive understanding of the full range of such mechanisms. This knowledge can be used not only to inform the selection of the best possible partner drugs for future combination therapies but also to prioritise the development of drugs capable of overcoming existing clinical resistance. Here we report the characterisation of AmB-resistant *L. donovani* clones generated through *in vitro* selection. Whole genome sequencing revealed that in three moderately resistant clones (5-8-fold compared to wild-type), resistance was due solely to the deletion of the gene encoding C24-sterol methyltransferase (SMT1). A fourth clone demonstrating the most significant levels of AmB resistance (>60-fold compared to wild-type) was found to be functionally null for a putative P450 reductase (P450R1). Sterol profiling indicated that P450R1 null parasites were deficient in sterol 14-alpha demethylase (CYP51) activity leading us to hypothesise that this putative reductase may be responsible for regeneration/reduction of CYP51. To our knowledge this represents the first time this putative P450R, which we now call P450 reductase 1 (P450R1), has been functionally characterised and implicated in AmB resistance. These studies expand our current understanding of the sterol biosynthetic pathway of *L. donovani*.

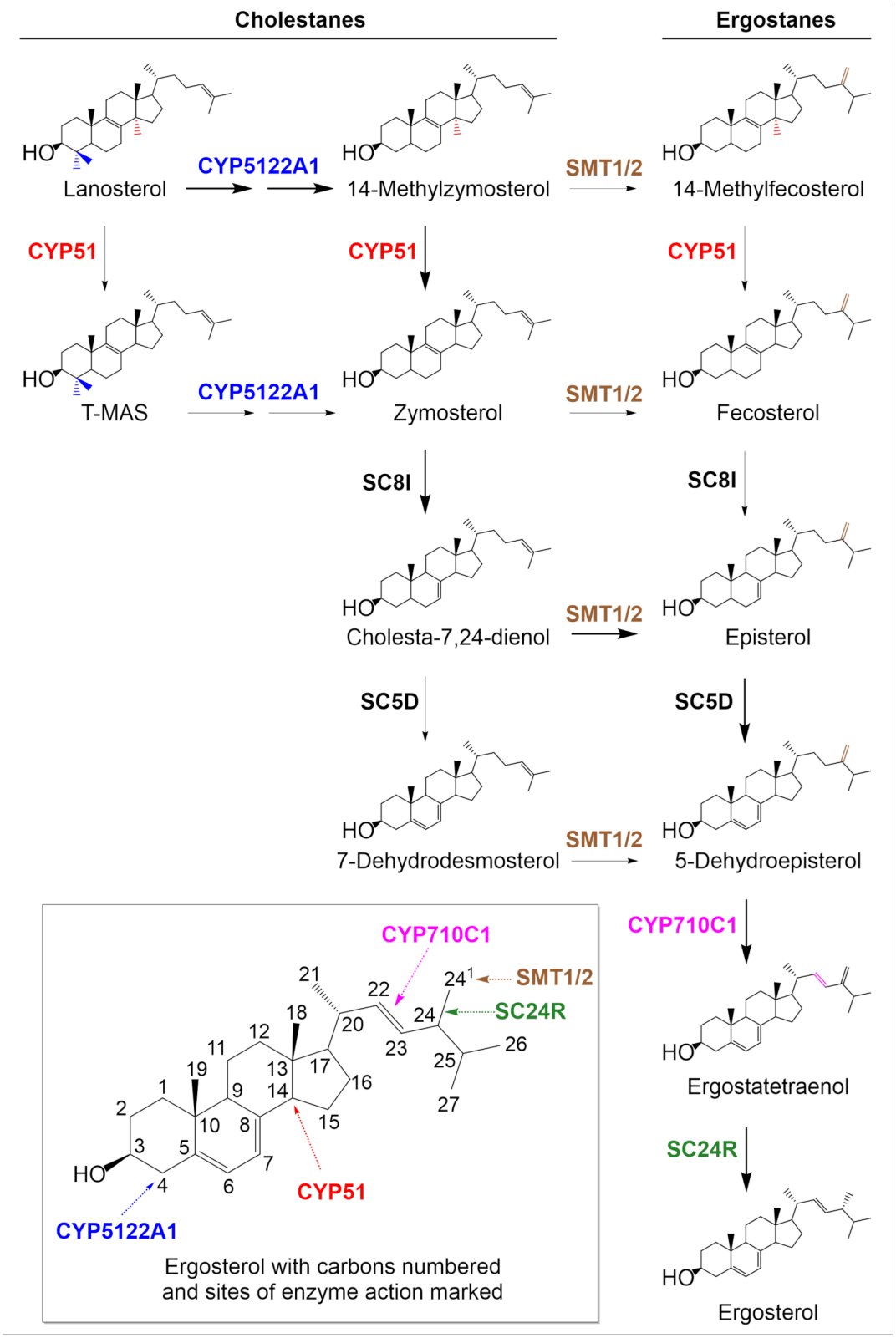

129 **Figure 1. *Leishmania* sterol biosynthetic pathway.**

Results and discussion

Resistance generation followed by whole genome sequencing

L. donovani promastigotes resistant to amphotericin B (AmB) were selected through *in vitro* evolution (**Figure 2**). Starting at 20 nM (1× EC_{50}), four drug-sensitive, clonal cell lines were exposed to stepwise increasing concentrations of AmB until they could grow at concentrations equivalent to >20× the established EC_{50} value (**Figure 2B**). The four independently generated resistant cell lines were cloned by limiting dilution, and the susceptibility of the resulting clones to AmB was assessed. Three of the clones (AmB R2, 3 and 4) were between 5- and 8-fold less sensitive to AmB than the wild-type (WT) parental clone (**Figure 2C** and **Table 1**). However, AmB R1 demonstrated considerably higher levels of resistance at >60-fold less susceptible to the drug. In each case, resistance demonstrated by each clone was found to be relatively stable over at least 30 passages in culture in the absence of compound (**Table 1**).

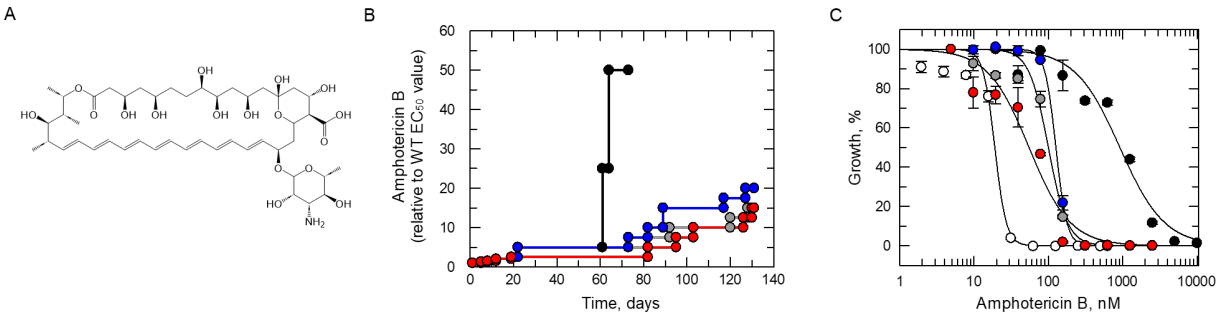

Figure 2. *In vitro* evolution of AmB resistance in *L. donovani*. (A) Chemical structure of amphotericin B. (B) Schematic representation of the generation of AmB-resistant cell lines in *L. donovani*. Each passage of cells in culture (circles, lines 1-4) is indicated with cell lines 1–4 indicated in black, grey, blue, and red, respectively. (C) Dose-response EC_{50} values for AmB were determined for WT (white) and cloned resistant cell lines 1–4 (black, grey, blue, and red, respectively). These representative curves are the nonlinear fits of data using a two-parameter EC_{50} equation provided by GraFit. An EC_{50} value of 19 ± 2 nM was determined for AmB against WT promastigotes. EC_{50} values for resistant clones AmB R1–4 were 915 ± 118, 100 ± 8, 126

± 0.8 and 55 ± 8 nM, respectively. These EC_{50} values represent one biological replicate, composed of two technical replicates. Collated datasets reporting the weighted mean ± SD of multiple biological replicates are summarised in **Table 1**.

Genomic DNA recovered from the four resistant clones was analysed by whole genome sequencing (WGS) (**Table S1**). The three cell lines demonstrating comparatively modest levels of resistance to AmB (AmB R2–4) were all found to maintain an additional copy of chromosome 26, compared to the parental WT clone (**Table S2**). Perhaps most notably, all three clones possessed deletions within the same sterol C24-methyl transferase (SMT) locus previously associated with AmB resistance [25, 26]. This locus is comprised of a tandem array of two near-identical transferase genes, *SMT1* (LdLV9.36.2.209980) and *SMT2* (LdLV9.36.2.209990) that differ by a single amino acid at position 321 (valine in SMT1 and isoleucine in SMT2). Sequence analysis enabled us to confirm that both copies of *SMT1*, as well as the intergenic region between *SMT1* and *2* genes, were deleted from cell lines AmB-R2 and R4 (**Figure 3A, Table S3**). In AmB R3, a homozygous 17-bp deletion was identified that introduced a premature stop codon into *SMT1*. As a representative of our *SMT1* deletion mutants, AmB R3 promastigotes were differentiated into axenic amastigotes and found to retain their AmB-resistant phenotype in this more medically relevant, mammalian stage of the parasite (**Table S4**).

In contrast, the hyper-resistant clone AmB-R1 maintained a full complement of *SMT1* and *2* genes (**Table S3**). CNV analysis confirmed that this clone lost a copy of chromosome 22, reducing the chromosome level from tetraploid to triploid (**Table S2**). We reasoned that reducing the dosage of genes on chromosome 22 by 25% would be unlikely to drive a >50-fold shift in drug susceptibility. AmB R1 maintained a total of eight mutations (**Table S1**). Five of these mutations were shared with one or more of the cell lines demonstrating modest AmB-resistance and therefore deemed unlikely to be responsible for hyper-resistance in AmB R1. Three mutations unique to AmB R1 were identified including a heterozygous 10 bp deletion in a gene (LdBPK_312290.1) encoding a hypothetical protein unique to *Leishmania spp*, a 69

bp heterozygous insertion within the gene (LdBPK_360990.1) encoding the 40S ribosomal protein S18 and a homozygous 24 bp deletion within a gene (LdBPK_281350.1) encoding a putative cytochrome P450 reductase (also known as a haemoprotein reductase, P450R1) (**Figure 4A**). Since P450Rs, are known to play a key role in sterol biosynthesis and drug metabolism [30], we sought to further investigate the role of this INDEL in AmB hyper-resistance alongside the role of *SMT1* deletion in moderate resistance.

Investigating the role(s) of SMT1 and SMT2 in AmB resistance

SMTs catalyse the methylation of the C24 side chain of cholestanes to form the cognate ergostane (**Figure 1**). Broadly speaking, organisms that maintain both SMT1 and SMT2 enzymes produce both C24-methylated and -ethylated sterols while those possessing only SMT1 produce C24-methylated sterols. Expression of *Nicotiana tabacum* SMT1 in SMT1-deficient *Saccharomyces cerevisiae* resulted in the production of C24-methylated sterols, while expression of SMT2 in these SMT1-deficient yeast resulted in the production of C24-ethylated sterols [31]. Thus, SMT1 is capable of catalysing the addition of a single methyl group while SMT2 can catalyse sequential methylation of sterols [32]. Dissection of the individual roles of *SMT1* and *SMT2* gene products in *Leishmania* has not yet been ascertained, but the conservation of the two genes across *Leishmania species* indicates they have distinct functions.

To interrogate the role of SMTs in AmB resistance, multiple transgenic cell lines were generated. In the first instance, we focused on the role of *SMT1* deletion in the modest resistance demonstrated by AmB R2–4. An ectopic copy of *SMT1* was re-introduced into AmB R3 via the *Leishmania*-specific expression vector pIR1 [33]. Successful re-introduction of SMT1 into AmB R3 was confirmed by quantitative proteomics (**Figure S3A**) and found to restore AmB-sensitivity to these formerly resistant promastigotes (**Figure 3B, Table 1**). In addition, sequential knock-out of *SMT1* from WT cells by CRISPR-Cas9 gene editing,

confirmed by WGS (**Table S3**)), resulted in promastigotes (*SMT1* DKO) that were 8-fold less susceptible to AmB, a similar level of resistance demonstrated by AmB R2–4. *SMT1* DKO promastigotes readily differentiated into axenic amastigotes and remained resistant to AmB in this developmental form (**Table S4**). Collectively, these data confirm the causal link between SMT1 functional loss and AmB resistance in our moderately resistant *L. donovani* promastigote cell lines and are entirely consistent with previous observations in *L. mexicana* [25, 26], and some earlier report in *L. donovani* [14, 34-36].

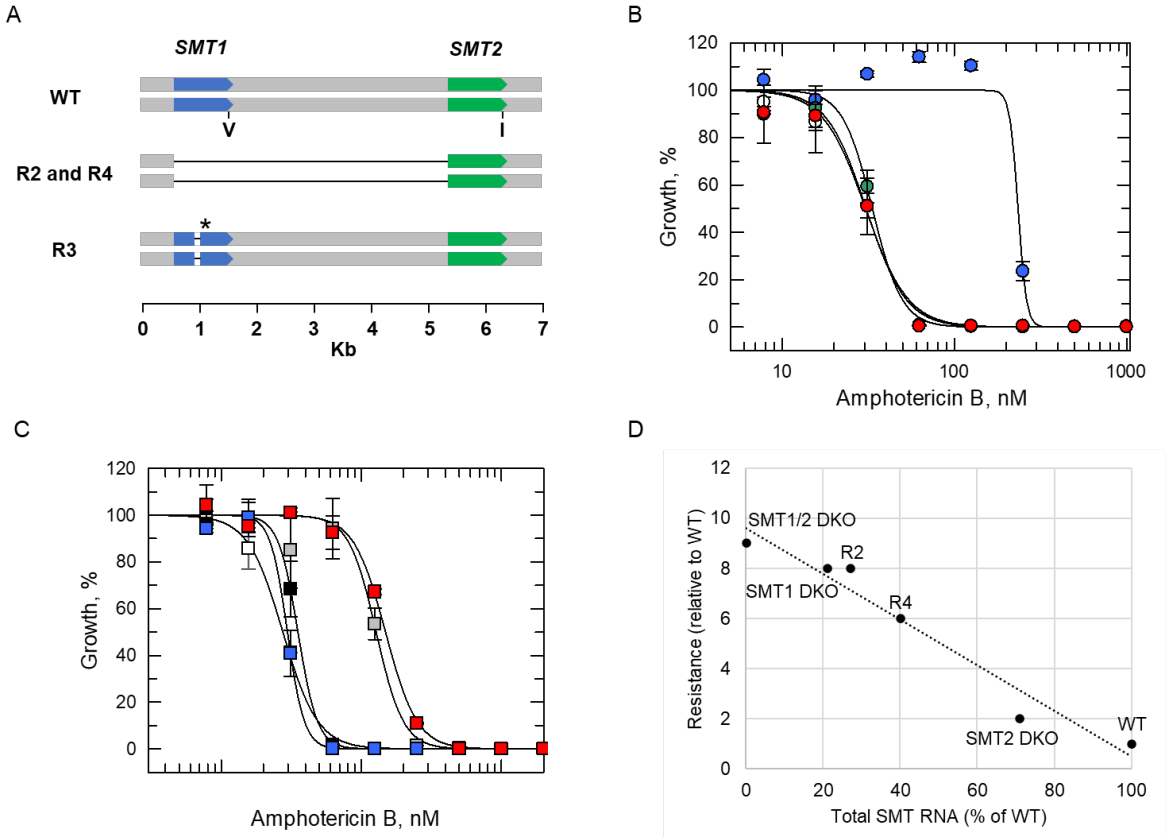

Figure 3. Investigating the impact of *SMT1* and *SMT2* deletions on AmB susceptibility. (A) Schematic representation of *SMT1*-related deletions identified in AmB R2–4 cell lines. The site of the single amino acid change between SMT1 (V indicating valine) and SMT2 (I indicating isoleucine are shown. The site of the new stop codon in AmB R3 is denoted by an asterisk. (B) Dose-response curves for WT (white), AmB R3 (blue), AmB R3 plus *SMT1*^{WT} add-back (green) and AmB R3 plus *SMT2*^{WT} add-back (red) clones treated with AmB. EC_{50} values of 30 ± 1, 234 ± 36, 33 ± 2 and 31 ± 1 nM were determined for WT, AmB R3, AmB R3

plus *SMT1*^{WT} add-back and AmB R3 plus *SMT2*^{WT} add-back promastigotes, respectively. (C) Dose-response curves for WT (white), *SMT1* SKO (black), *SMT1* DKO (grey), *SMT2* DKO (blue), and *SMT1/2* DKO (red) EC_{50} values of 28 ± 1, 35 ± 1, 128 ± 6, 30 ± 0.6 and 149 ± 4 nM were determined for WT, *SMT1* SKO, *SMT1* DKO, *SMT2* DKO, and *SMT1/2* DKO promastigotes, respectively. These EC_{50} curves and values represent one biological replicate, composed of two technical replicates. Collated datasets reporting the weighted mean ± SD of multiple biological replicates are summarised in **Table 1**. (D) Plot of total *SMT* RNA versus level of AmB resistance, relative to WT.

Since SMT1 and 2 are virtually identical, except for of a single amino acid substitution, we investigated the potential role of SMT2 in AmB susceptibility and/or resistance. In the first instance, we overexpressed SMT2 in AmB R3 (**Figure S3**). Overexpression of this putative methyltransferase reverted AmB resistance in R3 promastigotes (**Table 1**) and axenic amastigotes (**Table S4**) indicating that SMT2 can functionally complement SMT1. Next, both gene copies of *SMT2* were deleted from WT parasites via CRISPR-Cas9 gene editing, with deletion confirmed by WGS (**Table S3**). However, removal of both *SMT2* gene copies from WT had little or no impact on levels of AmB resistance (**Table 1, Table S4 and Figure 3C**). A ransgenic cell line was then generated where both *SMT1* and *2* genes were simultaneously deleted (SMT1/2 DKO). Deletion of both *SMT1* and *2* did not markedly affect the growth rate of the resulting transgenic cell line confirming that both transferases are not required for either *L. donovani* promastigote or axenic amastigote viability. The resulting *SMT* null cell line demonstrated only marginally enhanced AmB resistance compared to our *SMT1* double knock-out (DKO) parasites (AmB susceptibility reduced by 10-fold versus 8-fold relative to WT).

Previous studies have reported that *SMT1* RNA levels are substantially higher than those of SMT2 in *L. donovani* [34] and *L. mexicana* [25]. Using quantitative RT-PCR, total *SMT* transcript levels in WT, SMT1 and SMT2 DKO cell lines were determined and compared (**Figure S1**). In SMT1 null promastigotes, total *SMT* transcript levels were ~70% lower than

measured in WT cells while transcript levels in SMT2 null parasites were ~30% lower. Prompted by these observations, we then measured *SMT* transcript levels in resistant cell lines (AmB R2–4) and plotted against AmB resistance (relative to WT). Levels of AmB resistance were found to inversely correlate to *SMT* transcript levels in these clones with an R^2 value of 0.95 (**Figure 3D**). Thus, modulating overall SMT enzyme activity can directly impact AmB susceptibility in *L. donovani*. Our data also indicates that SMT1 is more highly expressed and is likely the dominant SMT, thus explaining the profound impact of *SMT1* deletion on AmB resistance compared to *SMT2* deletion. Subsequent quantitative proteomics analysis of SMT levels in SMT1 and SMT2 DKO promastigotes confirm this observation with SMT1 expression levels again higher than SMT2 (**Figure S3A**).

Previous studies in *L. donovani* have demonstrated that while promastigotes synthesise only ergosterol (C24-methylated), axenic amastigotes synthesise both ergosterol and stigmasterol (C24-ethylated) [37]. This led us to hypothesise that, as is the case in other organisms, SMT2 may be responsible for synthesis of C24-ethylated sterols and that SMT2 may be predominantly expressed in the more medically relevant amastigote stage of the parasite. However, quantitative RT-PCR analysis of total *SMT* transcript levels in SMT1 and 2 null axenic amastigotes revealed that SMT1 accounts for >60% of the total *SMT* transcripts in these parasites (**Figure S2**), essentially replicating our promastigote data, with quantitative proteomics analysis confirming this observation at the protein level (**Figure S3A**). In addition, *SMT2* null axenic amastigotes remain susceptible to AmB (**Table S4**). It is possible that the observed low levels of SMT2 expression are sufficient to account for the C24-ethylated stigmasterol previously detected in amastigotes [37] but under these circumstances we would also expect to detect stigmasterol in promastigotes. While SMT2 expression levels are lower than SMT1, particularly in axenic amastigotes (**Figure S3B**), the fact that we can detect SMT2 expression and that overexpression can complement for SMT1 loss at both stages of the parasite, confirms that *SMT2* encodes a functional methyltransferase. We acknowledge that axenic amastigotes are not a perfect model for this critical stage of the parasite lifecycle and

future studies will focus on measuring SMT expression levels in more physiologically relevant amastigotes recovered from infected macrophages.

Investigating the association between P450R1 and AmB hyper-resistance

To determine if loss of P450R1 full length expression plays a direct and/or significant role in the hyper-resistant phenotype of AmB R1, an ectopic copy of this reductase was reintroduced into the cell line. Successful expression of P450R1 in these resistant parasites was confirmed by quantitative proteomics (**Figure S3C**). Adding back this functional copy of *P450R1* restored AmB susceptibility to almost WT levels. However, introducing an ectopic copy of *P450R1* bearing the 24-bp INDEL (Δ605-612) identified in AmB1 parasites failed to rescue drug susceptibility (**Table 1, Figure 4B**). Next, we utilised CRISPR-Cas9 gene editing to replicate the *P450R1* homozygous INDEL in WT promastigotes. Successful deletion of the 24-bp from both copies of *P450R1* was confirmed through Sanger sequencing, and the resulting clones were assessed to establish their susceptibility to AmB. Introduction of this INDEL into WT parasites induced hyper-resistance to AmB at a similar level to that demonstrated in our AmB R1 cell line (53-fold versus 63-fold shift, respectively, **Table 1, Figure 4C**). These data suggest that mutation of P450R1 is likely the primary driver for AmB hyper-resistance in AmB R1. To our knowledge, this represents the first time that a P450R has been implicated in resistance mechanisms to this clinical anti-microbial agent in either *Leishmania* or fungi.

We hypothesised that the 24-bp INDEL may have ablated P450R1 activity in AmB R1. To test this, we generated a P450R1 null cell line using CRISPR-Cas9 gene editing. The resulting transgenic parasites were hyper-resistant to AmB and at a similar magnitude to our AmB R1 cell line, with EC_{50} values shifting 64-fold relative to WT (**Table 1, Figure 4C**). These data confirm that P450R1 is not essential in *L. donovani* promastigotes and indicate that AmB R1 is almost certainly a functional null for P450R1. Notably, AmB R1 and P450R1 null cell lines could not be differentiated into axenic amastigotes, while both lines bearing a $P450R1^{WT}$

add-back could. In contrast, cell lines complemented with P450R1$^{\Delta 605\text{-}612}$ were unable to differentiate. We also assessed the ability of these cell lines to sustain an infection within primary macrophages. AmB R1, P450R1 DKO and add-back cell lines were grown in culture until they reached metacyclic promastigote stage. The resulting parasites were incubated with starch-elicited mouse peritoneal macrophages for 12 h. Non-phagocytosed promastigotes were removed and infected macrophages incubated for 72 h. The ability of AmB R1 and P450R1 DKO cell lines to establish and sustain an infection in primary macrophages was severely compromised, as determined by comparing the mean numbers of amastigotes per infected macrophage compared to WT (**Figure S5**). Adding back a functional copy of *P450R1* to DKO parasites restored infectivity to wild-type levels. However, addback of this gene did not restore infectivity to AmB R1. We hypothesise that this discrepancy may be due to P450R1-indepdendent changes that may have occurred within these parasites during prolonged resistance selection *in vitro*. Nevertheless, these data suggest that P450R1 is essential for both *L. donovani* amastigote viability and infectivity. Reassuringly, they also indicate that the hyper-resistant phenotype associated with AmB R1 could not be replicated in the clinic.

Analysis of sterol composition in AmB-resistant and transgenic promastigotes

It is widely accepted that the mechanism of action of AmB is principally through direct binding to, and sequestration of, ergosterol or related ergostane-type sterols [16, 21, 38]. Moreover, a multitude of studies have associated changes in sterol composition to AmB drug resistance in several organisms [25, 26, 34, 39]. Since the impact of SMT1 deletion on sterol composition has already been thoroughly investigated in *L. mexicana* [26], here we focused on profiling sterol changes induced by deletion of P450R1. Sterols within WT, AmB R1 and transgenic cell lines were profiled using gas chromatography-mass spectrometry (GS-MS) and identified based on retention time and spectral matches to established standards alongside comparison to the literature values (**Table S6**). The predominant sterols detected in our *L. donovani* WT

promastigotes were 5-dehydroepisterol (46.5 ± 0.9%), ergosterol (17.8 ± 1.0%), episterol (13.5 ± 0.7%) and cholesta-7,24-dienol (12.4 ± 0.8%), all ergostane-type sterols produced at the end of the *Leishmania* sterol biosynthetic pathway (**Figure 1**, **Figure 4D, Table S7)**. In contrast, vanishingly small quantities of these ergostane-type sterols were detected in AmB R1. Instead, our hyper-resistant parasites were enriched in 14-methylated sterols produced earlier in the biosynthetic pathway, namely C14-methylfecosterol (75.1 ± 0.4%), C14-methylzymosterol (9.9 ± 0.1%) and 4,14-dimethylzymosterol (5.5 ± 0.4%). As expected, introducing a functional copy of *P450R1* back into AmB R1 promastigotes was sufficient to restore WT sterol composition, while add back of *P450R1* bearing the previously described INDEL could not. The sterol profiles of the P450R1 DKO cell line, as well as the CRISPR-edited P450R1$^{\Delta 605–612}$ cell line, closely matched the profile of AmB R1 providing further evidence that deletion of amino acids 605–612 results in loss of P450R1 function.

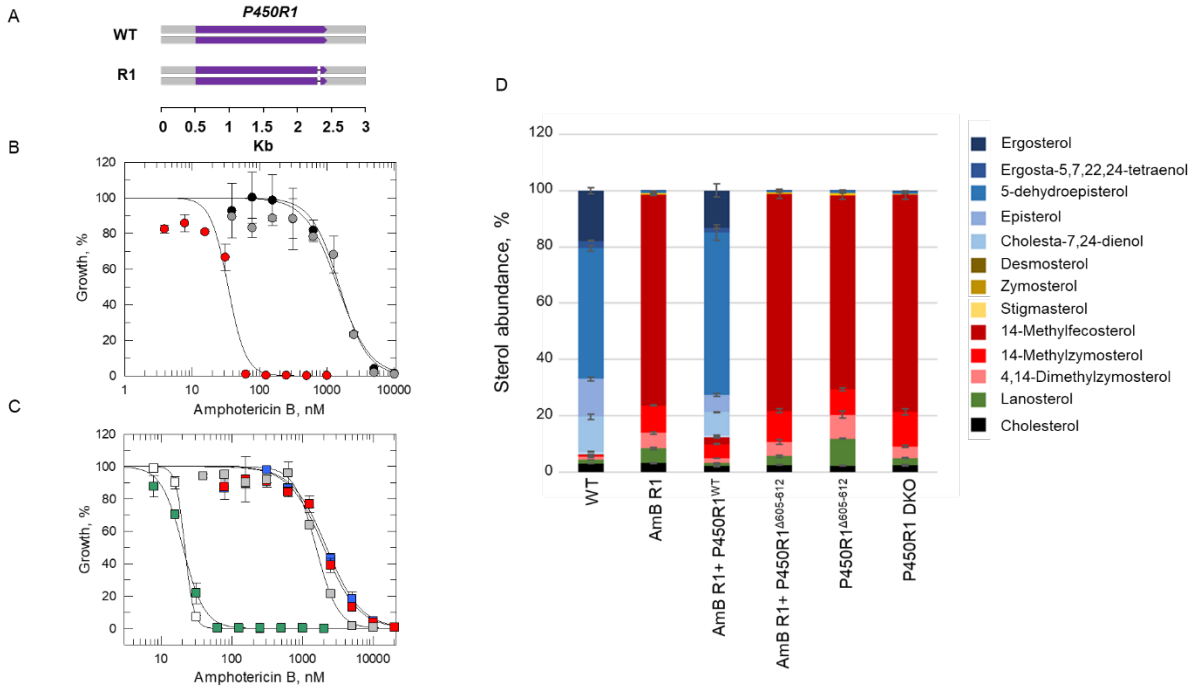

Figure 4: Investigating the impact of P450R1 functional loss on AmB susceptibility and sterol composition. (A) Schematic representation of the homozygous 24-bp deletion within *P450R1* in the AmB R1 cell line. (B) Dose–response curves for AmB-R1 (grey), AmB-R1 plus *P450R1*^{WT} add-back (red) and AmB-R1 plus *P450R1*$^{\Delta 605\text{-}612}$ add-back (black) promastigote

clones treated with AmB. EC_{50} values of 1530 ± 116, 34 ± 3.9, and 1450 ± 211 nM were determined for AmB-R1, AmB-R1 plus *P450R1*^{WT} add-back, and AmB-R1 plus *P450R1*$^{\Delta 605\text{-}612}$ addback, respectively. (C) Dose-response curves for WT (white), P450R1 DKO (blue), *P450R1* DKO plus *P450R1*^{WT} add-back (green), *P450R1* DKO plus *P450R1* $^{\Delta 605\text{-}612}$ add-back (red) and *P450R1*$^{\Delta 605\text{-}612}$ (grey) promastigotes treated with AmB. EC_{50} values of 22 ± 0.1, 2170 ± 204, 20 ± 0.7, 1990 ± 193 and 1550 ± 99 nM were determined for WT, *P450R1* DKO, *P450R1* DKO plus *P450R1*^{WT} add-back, *P450R1* DKO plus *P450R1*$^{\Delta 605\text{-}612}$ add-back and *P450R1*$^{\Delta 605\text{-}612}$ promastigotes, respectively. These EC_{50} curves and values represent one biological replicate, composed of two technical replicates. Collated datasets reporting the weighted mean ± SD of multiple biological replicates are summarised in **Table 1**. (D) Sterol profiling of WT and *P450R1* mutant promastigotes. Values are the mean ± SD from biological replicates.

Assessing the functional role of P450R1 in sterol biosynthesis

The loss of ergostane-type and accumulation of 14-methylated sterols in our various P450R1 null cell lines matches sterol profiles previously reported for CYP51 null *L. major* promastigotes [40], as well as promastigotes treated with azoles known to specifically inhibit CYP51 [41]. These observations led us to hypothesise that P450R1 may be responsible for regenerating CYP51 catalytic capacity in *L. donovani*. In contrast to human cells, which maintain a single NADPH-dependent cytochrome P450 reductase, three putative cytochrome P450 reductases have been identified in *L. donovani*. The focus of our current study, P450R1 and P450R2 (LdBPK_352600.1) share 35% sequence identity and 35% and 24% with human P450R, respectively. The remaining putative leishmanial P450R (P450R3, LdBPK_342500.1) more closely resembles the human NADPH-dependent diflavin oxidoreductase 1 (NDOR1), a central component of the cytosolic iron-sulphur (Fe-S) protein assembly machinery [42]. To our knowledge, specific functions have yet to be assigned to the three putative cytochrome P450 reductases in *Leishmania.* Alongside these reductases, *Leishmania* spp. maintain three cytochrome P450s (CYP51, CYP5122A1 and CYP710C1) that act at different points in the

371 sterol biosynthetic pathway (**Figure 1**). It is tempting to suggest that the three P450Rs have
372 specific roles, regenerating specific CYPs.

373 To explore the apparent association between P450R1 and CYP51, a *L. donovani* CYP51
374 DKO cell line was engineered. While knock-out of CYP51 has been achieved in *L. major* [40]
375 with the resulting parasites capable of infecting mice, previous attempts to generate CYP51-
376 null *L. donovani* were unsuccessful [43]. This led to speculation that CYP51 is indispensable
377 in *L. donovani* promastigotes and that CYP51-directed therapies should be considered for
378 visceral leishmaniasis [43]. Here, we were able to delete both copies of the CYP51 encoding
379 gene in a single round of CRISPR-Cas9 gene editing. Successful removal of both gene copies
380 was confirmed by WGS. The resulting *L. donovani* promastigotes did grow slower than WT
381 but could differentiate into axenic amastigotes and were able to infect mouse peritoneal
382 macrophages, albeit at a lower level than WT (**Figure S5**). These findings confirm that *CYP51*
383 is not essential for survival of *L. donovani*, at least *in vitro*, and that azoles known to target this
384 enzyme should not be considered for the treatment of visceral leishmaniasis. Consistent with
385 previous reports in *L. major* [40], CYP51 null *L. donovani* promastigotes were hyper-resistant
386 to AmB (**Table 1**). Next, we determined the sensitivity of our WT and (P450R1 and CYP51)
387 DKO cell lines to the established CYP51 inhibitor ketoconazole [44]. Drug susceptibility assays
388 with WT promastigotes exposed to ketoconazole resulted in a pronounced biphasic EC_{50} curve
389 with a lower EC_{50} value of 29 ± 5 nM and upper curve value of 5 ± 0.5 μM (**Figure 5, Table**
390 **S8**). Previous studies by Xu and colleagues proposed that lower concentrations of
391 ketoconazole (nM) are cytostatic for *L. major* promastigotes due to inhibition of non-essential
392 CYP51, but higher concentrations (>2 μM) are cytocidal through inhibition of an as yet
393 unidentified secondary target [40]. In support of this hypothesis, ketoconazole treatment of our
394 CYP51 nulls resulted in a canonical sigmoidal dose response curve (EC_{50} value – 5 ± 0.6 μM)
395 rather than a biphasic response. Notably, the response of P450R1-deficient promastigotes
396 (**Figure 5** and **Table S8**) to ketoconazole exposure closely mimicked that of the CYP51 nulls.
397 Collectively, these data demonstrate that CYP51 and P450R1 DKO cell lines phenocopy in

their responses to AmB and ketoconazole and is consistent with our hypothesis that P450R1 may be required for CYP51 activity.

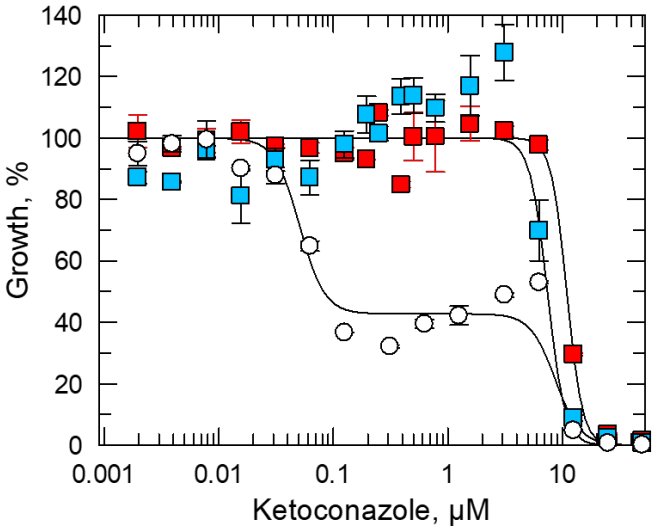

Figure 5: Investigating the impact of P450R1 and CYP51 functional loss on ketoconazole susceptibility. Dose–response curves for WT (white), CYP51 DKO (blue) and P450R1 DKO (red) promastigote clones treated with ketoconazole. EC_{50} values of 0.03 ± 0.01 (lower) and 10 ± 8 μM (upper) were determined for WT promastigotes while values of 11 ± 3 and 7 ± 1 μM were determined for P450R1 DKO and CYP51 DKO parasites, respectively. These EC_{50} curves and values represent one biological replicate, composed of two technical replicates. Collated datasets reporting the weighted mean ± SD of multiple biological replicates are summarised in **Table S8**.

The discrepancy in the essentiality between CYP51 and P450R1 indicates that P450R1 has functions in addition to its role in regeneration of CYP51 that are essential for amastigote viability. Indeed, P450R, also known as haemoprotein reductases, are likely to be involved in other redox functions. Future studies will aim to comprehensively characterise all functions of P450R1 as well as the other *Leishmania* P450 reductases.

Structural implications of the P450R1 INDEL

The structures of several P450R enzymes from a variety of species have been solved [45-48], with all sharing relatively similar architecture, comprised of FMN-, FAD- and NADPH-binding domains, as well as an *N*-terminal membrane anchor. The predicted AlphaFold structure of *Ld*P450R1 shares the same broad structure (**Figure 6**) [49, 50]. Crucially, the model is predicted with high to very high confidence, and the catalytic residues overlay with those of the human enzyme [45]. Following binding of NADPH, electrons are transferred sequentially to FAD and then FMN, which are closely aligned for electron transfer while the enzyme is in its closed conformation. Electron transfer from NADPH to FMN induces a significant conformational change, ultimately driving the enzyme into an open conformation and creating the substrate (CYP) binding site [51]. The predominant P450R-CYP interaction is via the P450R FMN-binding domain, however, molecular dynamic simulations indicate that final helix of the NADPH-binding domain (helix 21) also interacts directly with CYP [52]. Amino acids 605-612, deleted in AmB R1, are located on helix 20 which directly interacts with the CYP-binding helix 21, as well as helices 18 and 19 which form the NADPH biding site. We hypothesise that deletion of residues 605-612 and the resulting truncation of helix 20 will likely

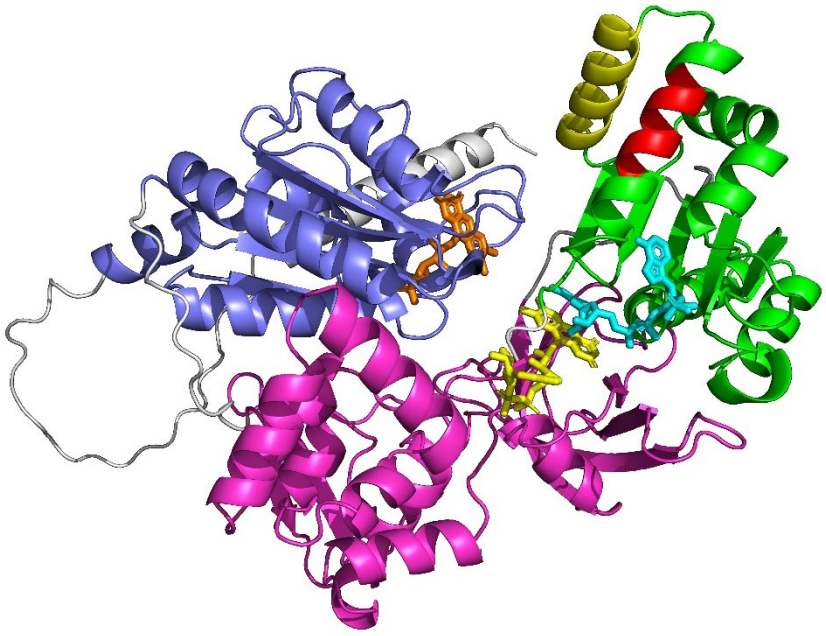

disrupt key interactions with neighbouring helices, thus impacting NADPH and/or CYP51 binding.

Figure 6: AlphaFold model of *Ld*P450R1 in closed conformation. The FMN, FAD and NADPH binding domains are highlighted in blue, magenta and green, respectively. The N-terminal membrane attachment domain is highlighted in grey. FMN (orange), FAD (yellow) and NADPH (cyan) are shown in stick representation with binding modes modelled from the rat P450R structure (1J9Z.pdb). Helix 21 (H21), known to directly interact with partner CYPs is highlighted in yellow. Amino acids 605-612, deleted in our AmB R1, form part of helix 20 (H20). Deleted amino acids are highlighted in red.

Conclusions

At the outset of these studies our principal goal was to add to the current understanding of AmB resistance mechanisms in *L. donovani*. In keeping with previous studies in *L. mexicana*, we confirmed that deletion of SMT1 was the primary driver of the moderate resistance demonstrated by three out of four of our cell lines. Comprehensive genetic and biochemical analysis of our remaining hyper-resistant clone confirmed that these parasites were deficient in P450R1, a *bona fide* P450 reductase likely involved in catalytic regeneration of CYP51. These studies contribute to our general understanding of the *L. donovani* sterol biosynthetic pathway and pave the way for further investigations to understand the specific functions of the two remaining and uncharacterised *L. donovani* P450Rs. The fact that P450R1 is apparently essential for amastigote viability suggests that functional loss of this reductase is unlikely to be a major cause of AmB clinical resistance. However, as an essential enzyme in a pathway that is already the focus of anti-trypanosomal drug discovery efforts, P450R1 may represent an interesting prospect for future chemotherapeutic intervention.

Acknowledgements and funding

This work was supported by the following Wellcome Trust grants: 203134/Z/16/Z and 218448/Z/19/Z. We would like to thank Liam Ferguson and other members of the Read lab for

assisting in the production of starch-elicited macrophages for this study. We would also like to thank the FingerPrints Proteomics facility at the University of Dundee.

Data availability

The authors confirm that all data underlying the findings are fully available without restriction. All data are either within the paper and Supporting Information files or deposited in publicly accessible databases such as PRIDE and National Centre for Biotechnology Information Sequence Read Archive. Bespoke code used in the analysis of our datasets is deposited in GitHub and archived in Zenodo.

Materials and methods

Cell lines and culture conditions

Clonal *Leishmania donovani Ld*BOB (derived from MHOM/SD/62/1SCL2D) was grown either as promastigotes or axenic amastigotes in media specific for each developmental stage [33]. Promastigotes were grown at 28ºC while axenic amastigotes were grown at 37°C in 5% CO_2.

Drug sensitivity assays

Drug sensitivity assays were carried out as previously described [53]. Data were processed using GRAFIT (version 5.0.4, Erithacus Software) and fitted to the 2-parameter equation shown below to determine the effective concentration inhibiting growth by 50% (EC_{50}), where *[I]* is the inhibitor concentration, and *m* is the slope factor. Experiments were performed in biological triplicates with the data presented as the weighted mean ± standard deviation.

$$y = \frac{100}{1 + \left(\frac{[I]}{EC_{50}}\right)^{m}}$$

Biphasic dose response curves were fitted to the following equation, where A% is the amplitude of the low EC_{50} value:

$$y = \frac{A\%}{1 + \left(\frac{[I]}{EC_{50Low}}\right)^{mLow}} + \frac{100 - A\%}{1 + \left(\frac{[I]}{EC_{50High}}\right)^{mHigh}}$$

Generation of amphotericin B-resistant clones

Amphotericin B-resistant clones were generated through continuous culture of a promastigote *L. donovani* wild-type, drug-sensitive clone in the presence of increasing concentrations of amphotericin B. Starting at 20 nM (equivalent to 1× EC_{50}), resistance was generated in 4 independent cultures, as previously described [53]. Once cultures were able to grow in concentrations of drug equivalent to 20× EC_{50}, parasites were cloned by limiting dilution, and a single clone from each culture was selected for further investigation.

493 **Whole genome sequencing and analysis**

494 Genomic DNA was isolated from WT and resistant clones via classical SDS-proteinase K-
495 phenol-chloroform extraction. Whole genomic sequencing was performed using a DNBseq
496 next-generation sequencing platform (Beijing Genomics Institute, Hong Kong). Sequencing
497 reads, each 120 base pairs in length, were processed through the OVarFlow pipeline (release:
498 May10_2021_BQSR) [54]. This pipeline was deployed within a Docker container and
499 executed on a high-performance computing (HPC) cluster. Variant calling was performed
500 against the LdBPK genome version 39 sourced from TriTrypDB [55] and augmented with the
501 maxi-circle sequence obtained from GenBank (Accession No. CP022652.1). Additionally, the
502 BAM files generated were utilised for variant calling via bcftools (formerly samtools [56]) (v
503 1.9).

504 Variant call format (VCF) files produced from these analyses underwent filtration using
505 a custom Python script, which was designed to exclude variants uniformly called across all
506 samples. This step was implemented to ensure the identification of unique variants specific to
507 resistant clones as compared to the WT. Microsoft Excel was then utilised for the visualization
508 and inspection of these VCF files, facilitating the identification of mutations. Mutation
509 acceptance criteria included a genotype quality score of at least 99, a minimum of 20
510 supporting genotype reads (DP value 20) and an overall quality score of no less than 1000.

511 Gene copy number variations were assessed based on their Reads Per Kilobase of
512 transcript, per Million mapped reads (RPKM) values. The bam files produced by the OVarFlow
513 pipeline were used to compute the RPKM values. RPKM values were calculated utilising the
514 rpkm function provided by the edgeR package (3.28.0) [57] in R, leveraging gene count data
515 obtained through featureCounts (1.6.4) [58]. Chromosome copy number variation was
516 visualised using the RPKM gene values.

517 For each WGS sample, the number of 120-bp reads containing the *SMT1*-specific
518 subsequence 5´-GCACGTACAAGGCGACGGAGGTTTTGGAGGAGGCTGCGGAA-3´ and
519 *SMT2*-specific subsequence 5´-

GCACGTACAAGGCGACGGAGATTTTGGAGGAGGCTGCGGAA-3´ were counted using a custom script implemented in Python and expressed as percentage of total SMT-specific reads. SMT1 and SMT2 RPKM values were adjusted by multiplying the total SMT RPKM by percentage SMT1 and SMT2. True SMT1 and SMT2 gene copy numbers were calculated by dividing their adjusted RPKM by the average RPKM for chromosome 36 and multiplying by chromosome 36 ploidy.

All WGS datasets have been deposited with the National Centre for Biotechnology Information Sequence Read Archive (NCBI SRA) under project code PRJNA994719. The code used in this project has been deposited in GitHub (https://github.com/mtinti/amphotericin_Ldonovani) and archived in Zenodo (https://zenodo.org/records/10567623).

Expression of SMT1 and P450R1 in AmB-resistant cell lines

The genes encoding sterol C24-methyltransferase 1 (*SMT1*, LdLV9.36.2.209980) and 2 (*SMT2*, LdLV9.36.2.209990) were PCR-amplified from *L. donovani* wild-type genomic DNA using primers LBT-032 and LBT-033 (**Table S5**) and Q5 polymerase (NEB), as per manufacturers' instructions. The full-length genes were inserted into the overexpression plasmid pIR1SAT via a *BglII* site. Similarly, the gene encoding the putative P450 reductase (*P450R*, LdBPK_281350.1) was amplified from genomic DNA harvested from wild-type and AmB R3 parasites using primers LBT-150 and LBT-151. The resulting wild-type and mutated genes were cloned into pIR1SAT via *Xma*I and *Xba*I restriction sites. Mid-log AmB R3, *SMT1/2* DKO, AmB R1 or *P450R1* DKO promastigotes (10^7) were transfected with 10 µg of pIR1-SMT1 or pIR1-P450R, respectively, as previously described [59]. The resulting cultures were selected with 100 µg/ml nourseothricin, and clones were isolated by limiting dilution.

Introduction of P450R INDEL in WT promastigotes

Nucleotides 1813–1836 of *P450R* (P450R Δ605-612) were deleted from *Ld*BOB WT parasites constitutively expressing Cas9 and T7 RNA polymerase yielding the P450R1$^{\Delta 605\text{-}612}$ cell line, as previously described [60, 61]. Briefly, the single guide RNA (sgRNA) directing Cas9 to nucleotide 1834 was generated through PCR-extension of primer LBT-153 with primer G00, using the protocol established by Gluenz and colleagues [61]. The resulting sgRNA alongside the accompanying repair template (LBT-152) were transfected into promastigotes simultaneously, as described [59].

Generation of gene knockouts

Gene knockouts were engineered using CRISPR-Cas9. Briefly, two sgRNAs were generated targeting the 5´ and 3´ regions of the target genes (*SMT1*, *SMT2* and *P450R*). Repair templates comprised of a resistance cassette flanked by 25 nucleotides homologous to the 5'- and 3'-UTR regions of target genes. All primers used for the generation of sgRNA and repair templates were designed using LeishGEdit ([62], http://www.leishgedit.net/Home.html).

Specifically, for the generation of *SMT1* SKO, sgRNA templates directing Cas9 cleavage 5´ and 3´ to the *SMT1* gene were generated through PCR-extension of primers LBT-036 and LBT-037 respectively with primer G00. A puromycin KO cassette repair template was generated through PCR-amplification of pTPuro_v1 [61] with LBT-034 and LBT-035. Transfected cells were selected with 20 µg/ml puromycin, and clonal parasites were generated by limiting dilution. *SMT1* DKO parasites were generated by repeating this process with confirmed SKO cells, using the same sgRNA templates. However, in this instance the repair template was generated through PCR-amplification of pTBlast_v1 [61] with primers LBT-034 and LBT-035. Transfected SKO promastigotes were selected with 20 µg/ml puromycin and 10 µg/ml blasticidin, and clonal DKO parasites were isolated by limiting dilution.

All other DKO lines described were generated following a single round of transfection. For SMT2 (LdLV9.36.2.209990), sgRNA templates were generated through PCR-extension of primers LBT-040 and LBT-041 respectively with primer G00, and the repair templates were generated through PCR-amplification of pTPuro_v1 and pTBlast_v1 with primers LBT-038 and

LBT-039. For SMT1 and 2 dual KO, sgRNA templates were generated through PCR-extension of primers LBT-036 and LBT-041 respectively with primer G00, and the repair templates were generated through PCR-amplification of pTPuro_v1 and pTBlast_v1 with primers LBT-034 and LBT-039. For P450R (LdBPK_281350.1), sgRNA templates were generated through PCR-extension of primers LBT-156 and LBT-157 respectively with primer G00, and the repair templates were generated through PCR-amplification of pTPuro_v1 and pTBlast_v1 with primers LBT-154 and LBT-155. For CYP51 (LdBPK_111100.1), sgRNA templates were generated through PCR-extension of primers LBT-169 and LBT-170 respectively with primer G00, and the repair templates were generated through PCR-amplification of pTPuro_v1 and pTBlast_v1 with primers LBT-167 and LBT-168.

For each DKO cell line, relevant sgRNA and repair templates were combined and transfected into WT *L. donovani* promastigotes constitutively expressing Cas9 and T7 RNA polymerase, as described above. Transfected cells were selected with 20 μg/ml puromycin and 10 μg/ml blasticidin 24 h following transfection. Clonal parasites were generated for each line by limiting dilution and confirmed as null for our genes of interest by whole genome sequencing.

Quantitative RT-PCR

RNA was harvested from 10^8 promastigotes using the RNeasy kit (Qiagen) according to the manufacturer's instructions. Residual DNA was digested from samples with RNase-Free DNase (Qiagen). Quantitative RT-PCR was performed with 100 ng of total RNA using a Luna Universal One-Step RT-qPCR kit (New England Biolabs) as previously described [63]. Relative quantification was established using the established reference gene rRNA45 [64]. Primers were designed using the Primer3Plus website. For total *SMT* RNA quantitation, primers LBT-090 and LBT-091 were used, and for P450R RNA quantitation primers LBT-177 and LBT-178 were used. The levels of each RNA transcript in AmB-resistant and transgenic clones were normalised to WT using the ΔΔCT method. Two biological replicates were performed for each analysis.

Quantitative proteomics

Sample preparation - *L. donovani* cell lysates were prepared precisely as previously described [53]. Protein digests were processed using S-Trap (Protifi) according to the manufacturer's recommendations. Briefly, 50 µg protein was solubilised in 5% (v/v) SDS, reduced with 10 mM tris(2-carboxyethyl)phosphine (TCEP) for 15 min at 55 °C, alkylated with 40 mM iodoacetamide for 30 min at RT in the dark. Alkylated proteins were suspended in the presence of 2.5% H_3PO_4, captured on a S-Trap micro column where they were washed and then digested with Trypsin/LysC at 10:1 protein:enzyme ratio at 37 °C for ~16h. Peptides were eluted with a combination of aqueous and organic buffers and dried on a vacuum evaporator.

Mass spectrometry analysis - LC-MS/MS analysis was performed by the FingerPrints Proteomics Facility (University of Dundee) on a Orbitrap Astral mass spectrometer (Thermo Scientific) coupled with a Vanquish Neo HPLC (Thermo Scientific). LC buffers used were as follows: Buffer A (0.1% formic acid in Milli-Q water (v/v)) and Buffer B (80% acetonitrile and 0.1% formic acid in Milli-Q water (v/v). Aliquots (15 µl) were loaded at 60 µL/min onto a trap column (PepMap Neo C18 5 µm 300 µm x 5mm, Thermo Scientific) pre-equilibrated with 96% Buffer A. The trap column was washed for 5 min at 200 µL/min and then the trap column was switched in-line with a Thermo Scientific, resolving column (PepMap RSLC C18, 2µm, 150µm x15 cm). The peptides were eluted from the column at a constant flow rate of 1.3 µL/min with a gradient from 4% buffer to 22.5% Buffer B in 13.9 min, 35% B in 6.9 min, 55% B in 0.5 min and then 99% Buffer B by 21.7 min. The column was then washed with 99% Buffer B for 0.9 min and re-equilibrated in 4% Buffer B. The Orbitrap Astral was operated in positive mode using data-independent mode. A scan cycle comprised an Orbitrap MS1 scan (m/z range from 380-980, with a maximum ion injection time of 5 ms, a resolution of 240,000 and automatic gain control (AGC) value of 500% followed by 149 Astral DIA scans (with an isolation window set to 4 m/z, maximum ion injection time at 3 ms and AGC 500%). HCD collision energy was set to 25. To ensure mass accuracy, the mass spectrometer was calibrated on day one of analysis.

Data analysis - Protein search was performed in DIA-NN (version 1.8.1) using a library-free search. An *in-silico* library was generated using the *L. donovani* BPK282A1 proteome (UP000008980 from Uniprot.org). Searches included cabamidomethylation as a fixed modification and acetylation (*N*-terminus) and oxidation (methionine) as variable modifications. The match between runs option was active. All proteomics datasets have been deposited to the ProteomeXchange Consortium via the PRIDE partner repository under the identifier **PXD052472.**

Macrophage infectivity assays

In-macrophage infectivity assays were carried out using starch-elicited mouse peritoneal macrophages harvested from BALB/c mice and metacyclic promastigotes, as previously described [65].

Sterol profiling

Sterols were extracted from mid-log promastigotes (3×10^8 per sample) and analysed via GC-MS, as previously described [25]. Sterol-associated peaks in GC-MS data were assigned through direct matches to authentic sterol standards or through retention times and/or ion patterns associated with previously identified sterols [25] (details of each peak assignment summarised in **Table S6**). Sterols were then mapped to the *Leishmania* ergosterol biosynthesis pathway proposed by Zhang and co-workers ([41], **Figure 1**). Analysis was carried out on two biological replicates.

References

1. WHO. *Leishmaniasis*. Fact Sheets 2023; Available from: https://www.who.int/news-room/fact-sheets/detail/leishmaniasis.
2. Moore, E.M. and D.N. Lockwood, *Treatment of visceral leishmaniasis.* J Glob Infect Dis, 2010. **2**(2): p. 151-8.
3. Madusanka, R.K., H. Silva, and N.D. Karunaweera, *Treatment of Cutaneous Leishmaniasis and Insights into Species-Specific Responses: A Narrative Review.* Infect Dis Ther, 2022. **11**(2): p. 695-711.
4. Aldasoro, E., et al., *What to expect and when: benznidazole toxicity in chronic Chagas' disease treatment.* J Antimicrob Chemother, 2018. **73**(4): p. 1060-1067.
5. Soto, J. and P. Soto, *Miltefosine: oral treatment of leishmaniasis.* Expert Rev Anti Infect Ther, 2006. **4**(2): p. 177-85.
6. Croft, S.L., S. Sundar, and A.H. Fairlamb, *Drug resistance in leishmaniasis.* Clin Microbiol Rev, 2006. **19**(1): p. 111-26.
7. Rijal, S., et al., *Increasing failure of miltefosine in the treatment of Kala-azar in Nepal and the potential role of parasite drug resistance, reinfection, or noncompliance.* Clin Infect Dis, 2013. **56**(11): p. 1530-8.
8. Thakur, C.P., et al., *Do the diminishing efficacy and increasing toxicity of sodium stibogluconate in the treatment of visceral leishmaniasis in Bihar, India, justify its continued use as a first-line drug? An observational study of 80 cases.* Ann Trop Med Parasitol, 1998. **92**(5): p. 561-9.
9. Jha, T.K., et al., *Randomised controlled trial of aminosidine (paromomycin) v sodium stibogluconate for treating visceral leishmaniasis in North Bihar, India.* Bmj, 1998. **316**(7139): p. 1200-5.
10. Sundar, S., et al., *Comparison of short-course multidrug treatment with standard therapy for visceral leishmaniasis in India: an open-label, non-inferiority, randomised controlled trial.* Lancet, 2011. **377**(9764): p. 477-86.
11. Hailu, A., et al., *Geographical variation in the response of visceral leishmaniasis to paromomycin in East Africa: a multicentre, open-label, randomized trial.* PLoS Negl Trop Dis, 2010. **4**(10): p. e709.
12. Musa, A.M., et al., *Paromomycin for the treatment of visceral leishmaniasis in Sudan: a randomized, open-label, dose-finding study.* PLoS Negl Trop Dis, 2010. **4**(10): p. e855.
13. Sundar, S., et al., *Single-dose liposomal amphotericin B for visceral leishmaniasis in India.* N Engl J Med, 2010. **362**(6): p. 504-12.
14. Purkait, B., et al., *Mechanism of amphotericin B resistance in clinical isolates of Leishmania donovani.* Antimicrob Agents Chemother, 2012. **56**(2): p. 1031-41.
15. Eichenberger, A., et al., *A severe case of visceral leishmaniasis and liposomal amphotericin B treatment failure in an immunosuppressed patient 15 years after exposure.* BMC Infect Dis, 2017. **17**(1): p. 81.
16. Readio, J.D. and R. Bittman, *Equilibrium binding of amphotericin B and its methyl ester and borate complex to sterols.* Biochim Biophys Acta, 1982. **685**(2): p. 219-24.
17. Umegawa, Y., et al., *Amphotericin B assembles into seven-molecule ion channels: An NMR and molecular dynamics study.* Sci Adv, 2022. **8**(24): p. eabo2658.
18. te Welscher, Y.M., et al., *Natamycin blocks fungal growth by binding specifically to ergosterol without permeabilizing the membrane.* J Biol Chem, 2008. **283**(10): p. 6393-401.
19. Gray, K.C., et al., *Amphotericin primarily kills yeast by simply binding ergosterol.* Proc Natl Acad Sci U S A, 2012. **109**(7): p. 2234-9.
20. Anderson, T.M., et al., *Amphotericin forms an extramembranous and fungicidal sterol sponge.* Nat Chem Biol, 2014. **10**(5): p. 400-6.

21. Lewandowska, A., et al., *Fungicidal amphotericin B sponges are assemblies of staggered asymmetric homodimers encasing large void volumes.* Nat Struct Mol Biol, 2021. **28**(12): p. 972-981.
22. Maji, A., et al., *Tuning sterol extraction kinetics yields a renal-sparing polyene antifungal.* Nature, 2023. **623**(7989): p. 1079-1085.
23. Sanglard, D., et al., *Candida albicans mutations in the ergosterol biosynthetic pathway and resistance to several antifungal agents.* Antimicrob Agents Chemother, 2003. **47**(8): p. 2404-12.
24. Young, L.Y., C.M. Hull, and J. Heitman, *Disruption of ergosterol biosynthesis confers resistance to amphotericin B in Candida lusitaniae.* Antimicrob Agents Chemother, 2003. **47**(9): p. 2717-24.
25. Pountain, A.W., et al., *Genomic instability at the locus of sterol C24-methyltransferase promotes amphotericin B resistance in Leishmania parasites.* PLoS Negl Trop Dis, 2019. **13**(2): p. e0007052.
26. Alpizar-Sosa, E.A., et al., *Amphotericin B resistance in Leishmania mexicana: Alterations to sterol metabolism and oxidative stress response.* PLoS Negl Trop Dis, 2022. **16**(9): p. e0010779.
27. Mesa-Arango, A.C., et al., *The production of reactive oxygen species is a universal action mechanism of Amphotericin B against pathogenic yeasts and contributes to the fungicidal effect of this drug.* Antimicrob Agents Chemother, 2014. **58**(11): p. 6627-38.
28. Singh, K., et al., *Deciphering the interplay between cysteine synthase and thiol cascade proteins in modulating Amphotericin B resistance and survival of Leishmania donovani under oxidative stress.* Redox Biol, 2017. **12**: p. 350-366.
29. Sokol-Anderson, M.L., J. Brajtburg, and G. Medoff, *Amphotericin B-induced oxidative damage and killing of Candida albicans.* J Infect Dis, 1986. **154**(1): p. 76-83.
30. Manikandan, P. and S. Nagini, *Cytochrome P450 Structure, Function and Clinical Significance: A Review.* Curr Drug Targets, 2018. **19**(1): p. 38-54.
31. Bouvier-Navé, P., T. Husselstein, and P. Benveniste, *Two families of sterol methyltransferases are involved in the first and the second methylation steps of plant sterol biosynthesis.* Eur J Biochem, 1998. **256**(1): p. 88-96.
32. Husselstein, T., et al., *Transformation of Saccharomyces cerevisiae with a cDNA encoding a sterol C-methyltransferase from Arabidopsis thaliana results in the synthesis of 24-ethyl sterols.* FEBS Lett, 1996. **381**(1-2): p. 87-92.
33. Goyard, S., et al., *An in vitro system for developmental and genetic studies of Leishmania donovani phosphoglycans.* Mol Biochem Parasitol, 2003. **130**(1): p. 31-42.
34. Pourshafie, M., et al., *Cloning of S-adenosyl-L-methionine:C-24-Delta-sterol-methyltransferase (ERG6) from Leishmania donovani and characterization of mRNAs in wild-type and amphotericin B-Resistant promastigotes.* Antimicrob Agents Chemother, 2004. **48**(7): p. 2409-14.
35. Rastrojo, A., et al., *Genomic and transcriptomic alterations in Leishmania donovani lines experimentally resistant to antileishmanial drugs.* Int J Parasitol Drugs Drug Resist, 2018. **8**(2): p. 246-264.
36. Morelle, C., et al., *Well-Tolerated Amphotericin B Derivatives That Effectively Treat Visceral Leishmaniasis.* ACS Infect Dis, 2021. **7**(8): p. 2472-2482.
37. Bansal, R., et al., *Stigmasterol as a potential biomarker for amphotericin B resistance in Leishmania donovani.* J Antimicrob Chemother, 2020. **75**(4): p. 942-950.
38. Cavassin, F.B., et al., *Sixty years of Amphotericin B: An Overview of the Main Antifungal Agent Used to Treat Invasive Fungal Infections.* Infect Dis Ther, 2021. **10**(1): p. 115-147.
39. Navarro-Mendoza, M.I., et al., *Alternative ergosterol biosynthetic pathways confer antifungal drug resistance in the human pathogens within the Mucor species complex.* bioRxiv, 2023.
40. Xu, W., et al., *Sterol biosynthesis is required for heat resistance but not extracellular survival in leishmania.* PLoS Pathog, 2014. **10**(10): p. e1004427.

41. Feng, M., et al., *Sterol profiling of Leishmania parasites using a new HPLC-tandem mass spectrometry-based method and antifungal azoles as chemical probes reveals a key intermediate sterol that supports a branched ergosterol biosynthetic pathway.* Int J Parasitol Drugs Drug Resist, 2022. **20**: p. 27-42.
42. Finn, R.D., et al., *Identification of a functionally impaired allele of human novel oxidoreductase 1 (NDOR1), NDOR1*1.* Pharmacogenet Genomics, 2005. **15**(6): p. 381-6.
43. McCall, L.I., et al., *Targeting Ergosterol biosynthesis in Leishmania donovani: essentiality of sterol 14 alpha-demethylase.* PLoS Negl Trop Dis, 2015. **9**(3): p. e0003588.
44. Hargrove, T.Y., et al., *CYP51 structures and structure-based development of novel, pathogen-specific inhibitory scaffolds.* Int J Parasitol Drugs Drug Resist, 2012. **2**: p. 178-186.
45. Hubbard, P.A., et al., *NADPH-cytochrome P450 oxidoreductase. Structural basis for hydride and electron transfer.* J Biol Chem, 2001. **276**(31): p. 29163-70.
46. Niu, G., et al., *Structure of the Arabidopsis thaliana NADPH-cytochrome P450 reductase 2 (ATR2) provides insight into its function.* Febs j, 2017. **284**(5): p. 754-765.
47. Xia, C., et al., *Structural basis for human NADPH-cytochrome P450 oxidoreductase deficiency.* Proc Natl Acad Sci U S A, 2011. **108**(33): p. 13486-91.
48. Ebrecht, A.C., et al., *Biochemical and structural insights into the cytochrome P450 reductase from Candida tropicalis.* Sci Rep, 2019. **9**(1): p. 20088.
49. Jumper, J., et al., *Highly accurate protein structure prediction with AlphaFold.* Nature, 2021. **596**(7873): p. 583-589.
50. Varadi, M., et al., *AlphaFold Protein Structure Database: massively expanding the structural coverage of protein-sequence space with high-accuracy models.* Nucleic Acids Res, 2022. **50**(D1): p. D439-d444.
51. Freeman, S.L., et al., *Orchestrated Domain Movement in Catalysis by Cytochrome P450 Reductase.* Sci Rep, 2017. **7**(1): p. 9741.
52. Mukherjee, G., P.P. Nandekar, and R.C. Wade, *An electron transfer competent structural ensemble of membrane-bound cytochrome P450 1A1 and cytochrome P450 oxidoreductase.* Commun Biol, 2021. **4**(1): p. 55.
53. Paradela, L.S., et al., *Multiple unbiased approaches identify oxidosqualene cyclase as the molecular target of a promising anti-leishmanial.* Cell Chem Biol, 2021. **28**(5): p. 711-721.e8.
54. Bathke, J. and G. Luhken, *OVarFlow: a resource optimized GATK 4 based Open source Variant calling workFlow.* BMC Bioinformatics, 2021. **22**(1): p. 402.
55. Aslett, M., et al., *TriTrypDB: a functional genomic resource for the Trypanosomatidae.* Nucleic Acids Res, 2010. **38**(Database issue): p. D457-62.
56. Li, H., et al., *The Sequence Alignment/Map format and SAMtools.* Bioinformatics, 2009. **25**(16): p. 2078-9.
57. Robinson, M.D., D.J. McCarthy, and G.K. Smyth, *edgeR: a Bioconductor package for differential expression analysis of digital gene expression data.* Bioinformatics, 2010. **26**(1): p. 139-40.
58. Liao, Y., G.K. Smyth, and W. Shi, *featureCounts: an efficient general purpose program for assigning sequence reads to genomic features.* Bioinformatics, 2014. **30**(7): p. 923-30.
59. Wyllie, S., et al., *Activation of Bicyclic Nitro-drugs by a Novel Nitroreductase (NTR2) in Leishmania.* PLoS Pathog, 2016. **12**(11): p. e1005971.
60. Mowbray, C.E., et al., *DNDI-6148: A Novel Benzoxaborole Preclinical Candidate for the Treatment of Visceral Leishmaniasis.* J Med Chem, 2021. **64**(21): p. 16159-16176.
61. Beneke, T. and E. Gluenz, *LeishGEdit: A Method for Rapid Gene Knockout and Tagging Using CRISPR-Cas9.* Methods Mol Biol, 2019. **1971**: p. 189-210.
62. Beneke, T., et al., *A CRISPR Cas9 high-throughput genome editing toolkit for kinetoplastids.* R Soc Open Sci, 2017. **4**(5): p. 170095.
63. Lima, M.L., et al., *Identification of a Proteasome-Targeting Arylsulfonamide with Potential for the Treatment of Chagas' Disease.* Antimicrob Agents Chemother, 2022. **66**(1): p. e0153521.

64. Ouakad, M., et al., *Selection of endogenous reference genes for gene expression analysis in Leishmania major developmental stages.* Parasitol Res, 2007. **101**(2): p. 473-7.
65. Wyllie, S., S. Patterson, and A.H. Fairlamb, *Assessing the essentiality of Leishmania donovani nitroreductase and its role in nitro drug activation.* Antimicrob Agents Chemother, 2013. **57**(2): p. 901-6.

Supplementary information - contents

(C) P450R1 protein levels (relative to WT) in promastigotes. Details of these analyses can be found in the materials and methods.

Figure S4. Assessing the impact of *SMT1* and *SMT2* addback on AmB susceptibility. Dose-response curves for WT (white), SMT1/2 DKO (blue), SMT1/2 DKO plus $SMT1^{WT}$ add-back (green) and *SMT1/2* DKO plus $SMT2^{WT}$ add-back (red) promastigotes treated with AmB. EC_{50} values of 22 ± 0.1, 191 ± 2, 16 ± 0.01, and 18 ± 0.7 nM were determined for WT, *SMT1/2* DKO, *SMT1/2* DKO plus $SMT1^{WT}$ and *SMT1/2* DKO plus $SMT2^{WT}$ promastigotes, respectively. These EC_{50} curves and values represent one biological replicate, composed of two technical replicates. Collated datasets reporting the weighted mean ± SD of multiple biological replicates are summarised in **Table 1**.

Figure S5: Assessing the impact of modulating CYP51 and P450R1 levels on infectivity. Mean numbers of WT, DKO and resistant amastigotes infecting mouse peritoneal macrophages were determined following 72 h incubations. Bar represents the mean value of two biological replicates with the individual data points also shown.

846 **Table 1**: **Collated AmB EC_{50} values for WT, resistant and transgenic promastigote cell lines.**

Cell line	EC_{50} value, nM	Fold shift (relative to WT)	Biological replicates
WT	19 ± 0.1	-	8
AmB R1	1200 ± 91	63	8
AmB R2	148 ± 5	8	3
AmB R3	152 ± 1	8	8
AmB R4	88 ± 5	5	3
AmB R1 (p30)	816 ± 38	43	2
AmB R2 (p30)	107 ± 9	6	2
AmB R3 (p30)	181 ± 4	10	2
AmB R4 (p30)	88 ± 3	5	2
AmB R3 + $SMT1^{WT}$	28 ± 1	1	4
AmB R3 + $SMT2^{WT}$	33 ± 2	2	4
SMT1 SKO	36 ± 1	2	5
SMT1 DKO	143 ± 7	8	5
SMT2 DKO	31 ± 1	2	4
SMT1/2 DKO	187 ± 4	10	8
SMT1/2 DKO + $SMT1^{WT}$	16 ± 0.01	1	3
SMT1/2 DKO + $SMT2^{WT}$	23 ± 1	1	3
AmB R1 + $P450R1^{WT}$	42 ± 3	2	4

AmB R1 + P450R1^{MUT}	1880 ± 150	99	3
P450R$^{\Delta 605\text{-}612}$	1000 ± 65	53	6
P450R DKO	1211 ± 55	64	8
P450R DKO + P450R1^{WT}	26 ± 1	1	3
P450R DKO + P450R1^{MUT}	2758 ± 196	145	3
CYP51 DKO	3520 ± 240	185	8

847

848 $^{*}EC_{50}$ values represent the weighted mean ± standard deviation of the indicated number of biological replicates with each biological replicate
849 comprised of at least two technical replicates.

850